Micro-Masonry of MEMS Sensors and Actuators

Yong Zhang, Hohyun Keum, Kidong Park, Rashid Bashir, and Seok Kim

***Abstract*— Micro-masonry is a route to microassembly that involves elastomeric-stamp-based micromanipulation and direct bonding. This paper presents the assembly of MEMS mechanical sensors and actuators using micro-masonry, demonstrating its capability of constructing 3-D microdevices that are impossible or difficult to realize with monolithic microfabrication. Microfabrication processes for retrievable MEMS components (e.g., combs, spacers, and flexure beams) are developed. As micromanipulation tools, microtipped elastomeric stamps with reversible dry adhesion are also designed and fabricated to pick up and deterministically place those components. After the manipulation, the components are permanently bonded together via rapid thermal annealing without using any additional intermediate layers. The assembled MEMS device is modeled and analyzed in consideration of the microassembly misalignment. The sensing and actuating capabilities of the assembled MEMS devices are experimentally characterized. [2013-0149]**

***Index Terms*— Microassembly, pick and place, elastomeric stamps, direct bonding, micro-masonry.**

I. Introduction

PICK-AND-PLACE microassembly is capable of integrating separately fabricated components into microsystems with high flexibility and precision, representing a unique approach to constructing devices that are impossible to accomplish with microfabrication alone or other microassembly methods (e.g., self-assembly, vibration-driven assembly, and fluidic assembly). For example, individual microfabricated photonic plates were picked up and assembled together by a microprobe to form novel 3-D photonic crystals [1]. 3-D microstructures assembled by a microgripper were also demonstrated [2].

Analogous in function to the assembly in the macro world, pick-and-place microassembly can construct complex structures from heterogeneous components. Thus, it has the potential to not only build novel devices but also reduce the fabrication complexity of some existing ones. Nevertheless, there remain some challenges that hinder the development of this technology and also its application. Currently the manipulation tools available for pick-and-place microassembly are usually either single-ended microprobes or double-ended microgrippers. Owing to strong adhesion forces at the microscale (i.e., capillary forces, van der Waals forces, and electrostatic forces), each tool has severe shortcomings that are difficult to overcome.

Microprobes are widely used for micromanipulation because they are easy to fabricate, inexpensive, readily available on the market, and easy to set up. The adhesion forces between a microprobe and a microobject enable the pick-up of the microobject from its substrate, and afterward must be overcome for the release of the microobject to a target location. Specifically, the pick-up step requires the adhesion forces between the microprobe and the microobject to be larger than the adhesion forces between the microobject and its substrate, which is challenging due to the small contact area between the microprobe tip and the microobject. Pick-up techniques such as rolling the microobject on its substrate [3], [4], soldering the micro/nanoobject to the microprobe [5], [6], and using two microprobes in coordination [7]–[9] were attempted, but they are skill-dependent and entail repeated trial-and-error efforts.

Releasing a microobject from a microprobe to a desired location is even more challenging than the pick-up step, thereby having motivated the development of a number of release techniques. Depending on whether the release process requires physical contact between the microobject and the target substrate, those techniques can be classified into contact release techniques and non-contact release techniques. The former class includes rolling the microobject on the substrate surface [3], [4], coating the substrate with adhesives [10], [11], soldering the micro/nanoobject to the substrate [5], [6], scraping the microprobe against the substrate edge [12], and incorporating mating interfaces on the microobject and the substrate such as snap-lock [2], [13], [14] and slots [7]. The latter class includes applying a voltage between the microprobe and the substrate to electrostatically attract the microobject to the substrate [15], vibrating the microprobe [16], and impacting the microobject with another microprobe [17], [18].

MEMS microgrippers [2], [17]–[21] have also been developed for the pick-and-place operation, offering an advantage of secure gripping over microprobes during the microobject pick-up and transport. For the release, the aforementioned release techniques can also be applied. However, none of those release techniques is able to accurately place planar microfabricated structures without mating interfaces or adhesives.

In addition to the aforementioned pick-and-place techniques, a parts-transfer technique [22] has also been demonstrated for MEMS assembly. Microfabricated silicon

Manuscript received May 11, 2013; revised June 12, 2013; accepted July 8, 2013. Date of publication July 29, 2013; date of current version March 31, 2014. This work was supported by the Center for Nanoscale Chemical-Electrical-Mechanical Manufacturing Systems at the University of Illinois at Urbana-Champaign. Subject Editor E. S. Kim.

Y. Zhang, H. Keum, and S. Kim are with the Department of Mechanical Science and Engineering, University of Illinois at Urbana-Champaign, Urbana, IL 61801, USA (e-mail: yong.zhang@aerospace.gatech.edu; hkeum2@illinois.edu; skm@illinois.edu).

K. Park is with the Department of Electrical and Computer Engineering and the Micro and Nanotechnology Laboratory, University of Illinois at Urbana-Champaign, Urbana, IL 61801, USA (e-mail: park35@gmail.com).

R. Bashir is with the Department of Electrical and Computer Engineering, the Department of Bioengineering, the Department of Mechanical Science and Engineering, and the Micro and Nanotechnology Laboratory, University of Illinois at Urbana-Champaign, Urbana, IL 61801, USA (e-mail: rbashir@illinois.edu).

Color versions of one or more of the figures in this paper are available online at http://ieeexplore.ieee.org.

Digital Object Identifier 10.1109/JMEMS.2013.2273439

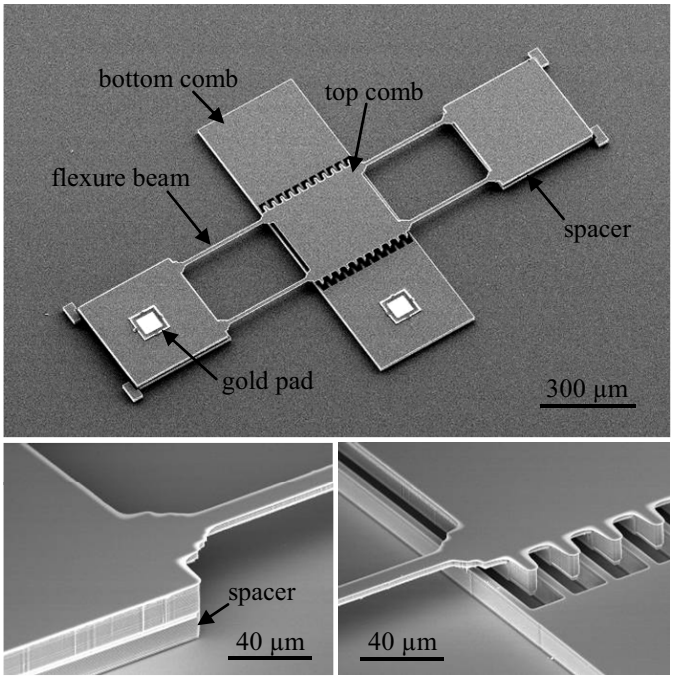

Fig. 1. SEM images of an assembled MEMS comb-drive device that is composed of a top comb, a bottom comb, two spacers, and two gold pads.

TABLE I
STRUCTURAL PARAMETERS OF THE COMB DRIVE

parameters	values
size of entire top comb	1740 μm × 350 μm × 20 μm
size of pads of top comb	350 μm × 350 μm × 20 μm
dimensions of flexure beams of top comb	350 μm (length) × 15 μm (width) × 5 μm (thickness)
dimensions of comb fingers of top comb	350 μm (length) × 10 μm (width) × 15 μm (thickness)
number of comb fingers of top comb	11
width of gap between adjacent comb fingers of top comb	22 μm
size of spacers	350 μm × 350 μm × 15 μm
size of entire bottom comb	1080 μm × 362 μm × 20 μm
dimensions of comb fingers of bottom comb	380 μm (length) × 10 μm (width) × 20 μm (thickness)
number of comb fingers of bottom comb	12
width of gap between adjacent comb fingers of bottom comb	22 μm
initial vertical overlap between top and bottom comb fingers	5 μm
width of gap between opposing comb fingers of top and bottom combs	6 μm
size of one of gold pads	100 μm × 100 μm × 0.3 μm

parts were transferred from a silicon substrate to a polydimethylsiloxane (PDMS) substrate that functioned as the assembly site, making use of the surface adhesion property of PDMS. However, it would be challenging to assemble multilayer silicon structures with strong bonding in between without the support of additional adhesive layers. Furthermore, any high temperature or corrosive processes are not allowed after the parts-transfer since they are incompatible with PDMS that was used as the structural material in the work [22].

Recently, a novel microassembly approach (termed micro-masonry) was developed [23]. Micro-masonry uses elastomeric stamps [24] as micromanipulation tools for pick-and-place microassembly and rapid thermal annealing for bonding of assembled materials. During the pick-and-place process, the adhesion forces between the manipulation tool and the microobject can be actively switched on and off to enable pick-up and release in a highly efficient manner. Previously, we have demonstrated the micro-masonry of three-dimensional structures from microscale silicon plates, blocks, and rings [23]. In this paper, we advance this micro-masonry technique further to address the long-standing challenge facing MEMS assembly. In comparison with our previous assembly of 3-D silicon microstructures [23], MEMS device assembly requires more complex and fragile structures such as combs and suspended flexure beams to be fabricated as retrievable components on a donor substrate and to be subsequently transferred to a receiver substrate. This paper reports the microfabrication processes for retrievable complex MEMS components and the microassembly processes for integrating those components into MEMS sensors and actuators. Furthermore, we demonstrate the integration of gold films onto the assembled silicon device via micro-masonry to form metal contacts and to facilitate a subsequent wire bonding process.

Fig. 1 shows the device constructed in this paper via micro-masonry. It is an out-of-plane vertical comb drive composed of a top comb, a bottom comb, two spacers, and two gold contact pads.

II. DESIGN AND FABRICATION OF MEMS COMPONENTS

The comb fingers of the top comb and bottom comb form a comb drive, as shown in Fig. 1. The comb drive can function as either an electrostatic actuator or a capacitive sensor. The dimensions and structural parameters of the device design are shown in Table I. The flexure beams have a length of 350 μm, a width of 15 μm, and a thickness of 5 μm. They are the most fragile portion of the top comb and may be fractured during the retrieval and placement of the top comb. Thus, the elastomeric-stamp-based manipulation of the top comb must consider the fragility of the flexure beams. The two gold pads have an area of 100 μm × 100 μm and a thickness of 0.3 μm, sufficiently large and thick for wire bonding to integrate the assembled device on printed circuit board (PCB). This vertical overlap between the top comb fingers and bottom comb fingers is initially 5 μm by design, to ensure that the comb drive operates in the linear range.

The top combs, bottom combs, and spacers are all fabricated from silicon-on-insulator (SOI) wafers.The top comb is fabricated from an SOI wafer with a 20-μm-thick device layer and a 1-μm-thick buried oxide (BOX) layer. The representative steps in the fabrication process of the top comb are illustrated in Fig. 2. First, 200-nm-thick silicon dioxide is thermally grown on the top side of the SOI wafer and is then patterned using reactive ion etching (RIE) to define comb fingers and two pads [Fig. 2(a)]. Subsequently, this silicon dioxide pattern and photoresist are used as two etch masks for a two-step deep reactive ion etching (DRIE) process to pattern the device layer

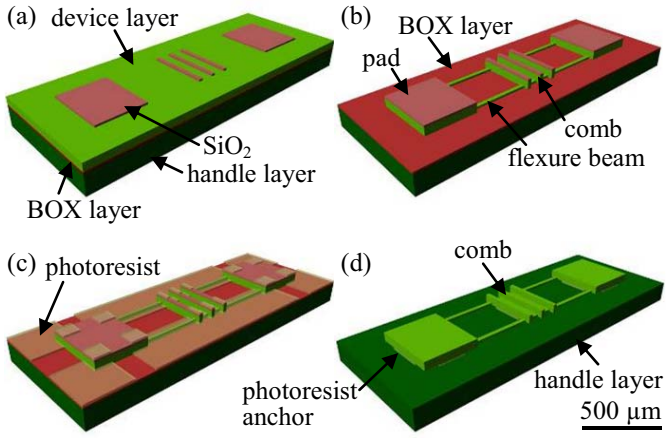

Fig. 2. Microfabrication process flow of top combs. (a) RIE of the top thermal oxide layer to pattern an etch mask. (b) Two-step DRIE of the device layer using thermal oxide and photoresist as two etch masks. (c) Photoresist patterning, followed by BOE to create undercuts below the device layer patterns. (d) HF etching after photoresist spinning and flood exposure to suspend the top comb on photoresist anchors.

to form four 5-μm-thick flexure beams, two pads, and comb fingers [Fig. 2(b)].

To make the top comb retrievable from its substrate, the following steps are used to suspend the top comb on photoresist anchors. Photoresist is spun and patterned [Fig. 2(c)] for the selective etch of the BOX layer using buffered oxide etch (BOE). When the exposed BOX layer is fully etched, there are approximately 1-μm-wide undercuts below the edges of the device layer patterns. After the photoresist removal, the top comb undergoes photoresist spinning again and flood exposure, leaving the photoresist remaining only at those undercut locations. Finally, HF is used to etch away the entire remaining BOX layer including the areas beneath the device layer patterns, resulting in the top comb suspended only on the photoresist anchors [Fig. 2(d)]. It can be seen from Fig. 2(c) that the photoresist covers the entire flexure beams, leading to the absence of photoresist anchors below the flexure beams, as shown in Fig. 2(d). The purpose of this design is to make the retrieval of the top comb facile without fracturing flexure beams.

With a similar process flow, the retrievable spacers are fabricated from an SOI wafer with a 15-μm-thick device layer and a 1-μm-thick BOX layer. The bottom comb does not require retrieval and is fabricated using one-step DRIE on an SOI wafer with a 20-μm-thick device layer and a 1-μm-thick BOX layer. The retrievable gold pads are fabricated from a gold thin film of 0.3 μm thick sputtered on a silicon dioxide layer on top of a silicon wafer. The fabrication details of the gold pads have been presented elsewhere [25].

III. Micro-Masonry Process

The retrievable components, i.e., spacers, top combs, and gold pads, need to be transferred from three different substrates where they are fabricated respectively to the bottom comb substrate to be assembled. Since the top comb must be aligned well ($\sim$1 μm accuracy) with the bottom comb during the assembly in order for the comb drive to function properly, a deterministic micromanipulation technique is required. The experimental setup for the microassembly processes includes x, y, z, and rotational mechanical stages and an optical microscope. The alignment precision of the setup is approximately 1 μm, satisfactory for the microassembly operation.

The reader is referred to [24] for the working principle of microtipped stamps. Briefly,when a microtipped stamp shown in Fig. 3(c2), is pressed against an object on a donor substrate, the region between microtips are mechanically collapsed, establishing a large contact area (corresponding to adhesion-on state), i.e., a high adhesion force, between the stamp and the microobject. Subsequently, the stamp is quickly retracted to retrieve the microobject, followed by the microtipped stamp returning to its initial shape due to an elastic restoring force. Thus, after the retrieval, the microobject is in contact with only the microtips, resulting in minimized adhesion at the stamp-microobject interface (corresponding to adhesion-off state). The microobject is then transferred to above a receiver substrate and lowered to establish the contact with the substrate. Finally, the stamp is slowly retracted, thereby delaminating the microtips from the microobject to complete the deterministic micromanipulation process.

It should be noted that the pick-and-place procedure is conducted on single components in this paper, rather than multiple components over a large area (e.g., wafer scale). Nevertheless, large-area assembly is possible through a parallel procedure using an array of microtipped stamps or a serial procedure using automated stages for high throughput, which remains as future work.

Here we extend this stamp-based technique to the assembly of MEMS components. As an example, the transfer process of the top comb is explained in detail below. The microtipped stamp designed to transfer top combs picks up a top comb, with the photoresist anchors remaining on the donor substrate [Fig. 3(a)]. It can be seen that the stamp has three sections to avoid its contact with the flexure beams; otherwise, the flexure beams may adhere to the sides of the microtips after the pick-up and fracture during the delamination for placing. After the pick-up, however, the comb fingers face inward to the stamp, making it impossible for them to mate with the bottom comb fingers. To flip over the top comb, it is transferred to a second microtipped stamp that is more adhesive than the first stamp [Fig. 3(b)]. Fig. 3(c1) and (c2) show the SEM images of the top comb on the second stamp. The degree of adhesiveness of a stamp can be controlled by two means: (i) altering the spacing between adjacent microtips in the stamp design; (ii) altering the mixing ratio of PDMS base and curing agent for the stamp molding.

In Fig. 3(d), the second stamp is approaching the bottom comb to place the top comb onto the two spacers that have already been assembled on the receiver substrate via micro-masonry. The resultant assembly is shown in Fig. 3(e1)(e2). To permanently bond the two pads of the top comb to the two spacers, the device is annealed at 1000 ^{o}C for 30 min for silicon fusion bonding. To facilitate the wire bonding from the device to a PCB, gold thin films are transferred and assembled

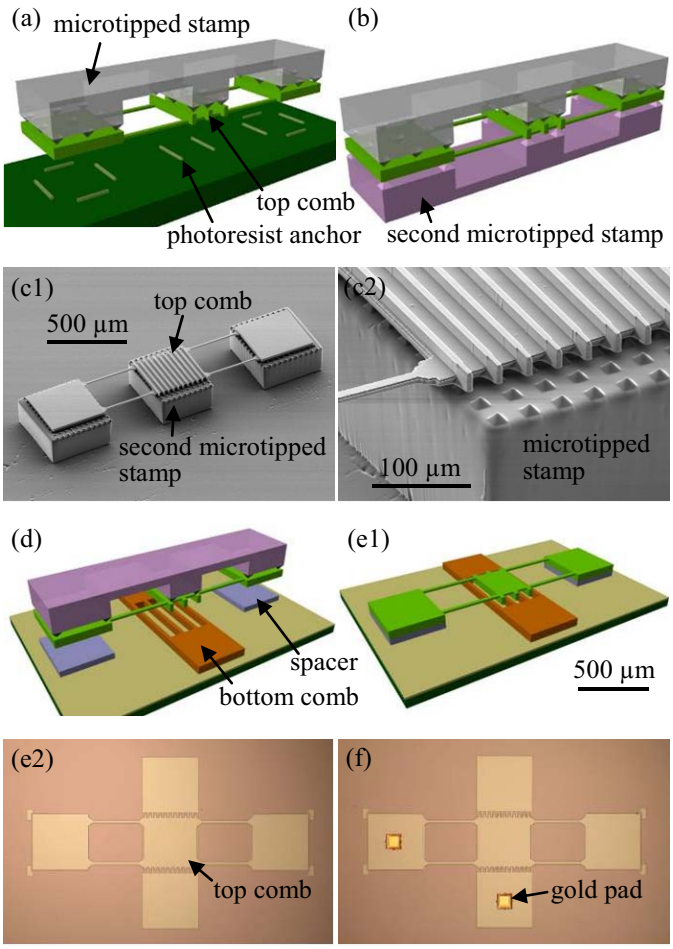

Fig. 3. Pick-and-place process of the top comb. (a) Pick-up of the top comb with a microtipped stamp from the donor substrate, with the photoresist anchors left. (b) Transfer of the top comb to another microtipped stamp to flip over the top comb to make the comb fingers face outward. (c1) SEM image of the top comb on the second stamp. (c2) Close-up SEM image of the comb fingers and microtipped stamp. (d) The stamp is approaching the bottom comb to print the top comb on the two spacers. (e1) The top comb is printed to form a comb drive. (e2) Optical microscopy image of the assembled comb drive. (f) Two gold pads are printed to facilitate wire bonding.

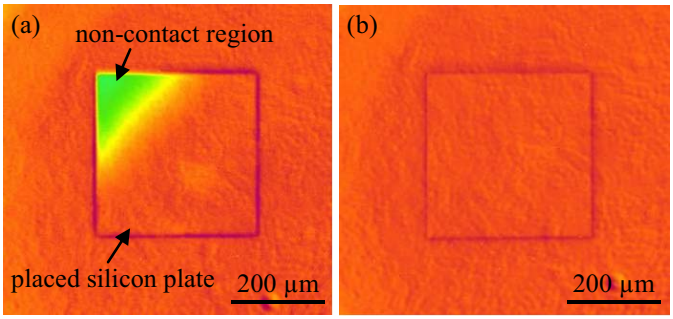

Fig. 4. Infrared transmission images of a silicon plate placed on a silicon substrate. (a) Prior to annealing, there is an noncontact region. (b) After annealing, the silicon plate is entirely bonded to the substrate.

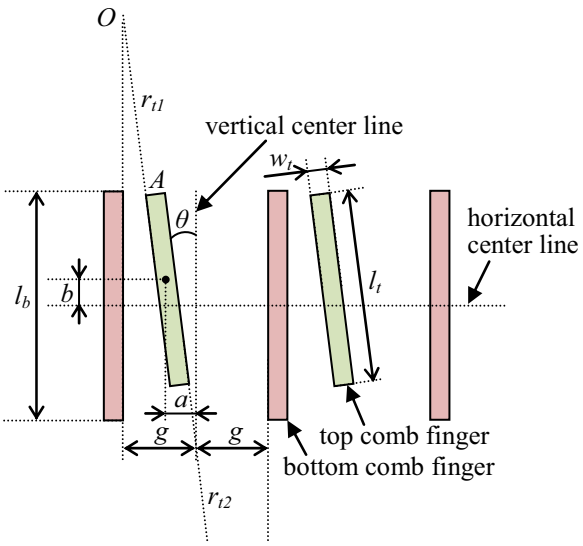

Fig. 5. Top view of the assembled comb drive for the capacitance calculation taking into account the translational misalignment (denoted by a and b) and angular misalignment (denoted by θ) of the top comb relative to the bottom comb.

to one pad of the top comb and one pad of the bottom comb, followed by annealing at 360 °C for 10 min to enhance their adhesion [Fig. 3(f)].

To investigate the effect and quality of the direct bonding, infrared transmission imaging is performed on a silicon plate placed onto a silicon substrate. Prior to the annealing, there is a weak-contact region, as shown in Fig. 4(a). However, that region disappears and the entire area of the silicon plate is bonded to the substrate after the annealing [Fig. 4(b)]. This test indicates that thermal annealing enhances uniform contact between the silicon plate and the silicon substrate, thereby enabling high quality direct bonding between them.

The capacitance between the top comb and bottom comb of the assembled device is modeled, in consideration of the translational and angular misalignments between the top comb and bottom comb, as illustrated in Fig. 5. The lengths of a bottom comb finger and a top comb finger are denoted by l_b and l_t, respectively. The translational and angular misalignments are denoted by (a, b) and θ, respectively. The width of a top comb finger is denoted by w_t. The upper extension of the left side of a top comb finger intersects with the extension of the bottom comb finger at point O, with an extension length of r_{t1}. Similarly, the lower extension of the right side of a top comb finger intersects with the extension of the bottom comb finger with an extension length of r_{t2}. The total capacitance between the top comb and bottom comb is [26]

$$C = n\,(C_1 + C_2) = n\left(\varepsilon\frac{p}{\theta}\ln\frac{l_t + r_{t1}}{r_{t1}} + \varepsilon\frac{p}{\theta}\ln\frac{l_t + r_{t2}}{r_{t2}}\right) \quad (1)$$

where n is the number of top comb fingers, C_1 (C_2) is the capacitance between a top comb finger and its left (right) adjacent bottom comb finger, ε is the permittivity of air, and p is the vertical overlap between the top comb and the bottom comb.

The electrostatic force between the top comb and the bottom comb at an applied voltage of V is

$$F = \frac{1}{2}\frac{dC}{dp}V^2 = \frac{1}{2}n\left(\frac{\varepsilon}{\theta}\ln\frac{l_t + r_{t1}}{r_{t1}} + \frac{\varepsilon}{\theta}\ln\frac{l_t + r_{t2}}{r_{t2}}\right). \quad (2)$$

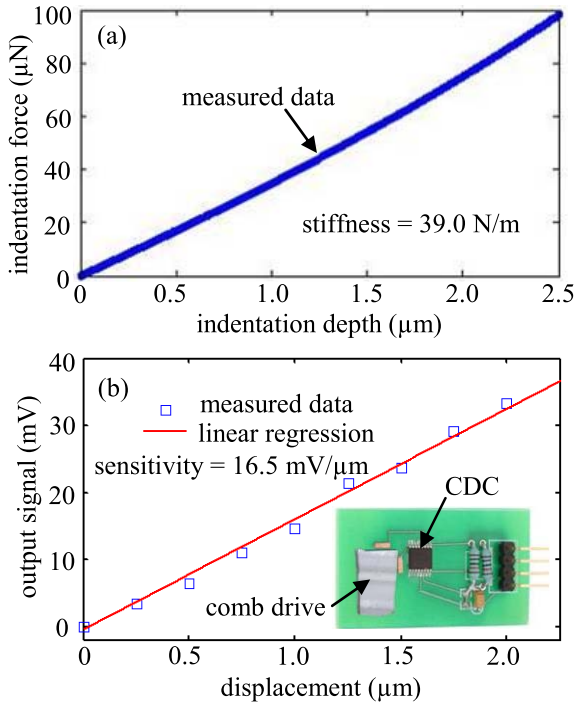

Fig. 6. Characterization of the comb drive as force and displacement sensors. (a) Stiffness was characterized via a nano indenter. (b) Capacitance-displacement relationship was characterized. Inset shows a device wire bonded to a circuit board with a capacitance-to-digital converter (CDC) for capacitive readout.

This force results in a top-comb displacement of

$$d = \frac{F}{k} = \frac{F}{4\frac{Ewt^3}{L^3}} \tag{3}$$

where k is the total spring constant of the four flexure beams, E is the Young's modulus of silicon, and w, t, and L are respectively the width, thickness, and length of a flexure beam.

The following comparisons are made to illustrate the effect of the misalignment (a, b, and θ) on the capacitance and the electrostatic force between the top comb and the bottom comb, using the structural parameters in Table I. With the assumption of no misalignment ($a = b = 0$ μm, $\theta = 0°$), the initial capacitance of the assembly is 56.8 fF. With the misalignment of a = 0.5 μm, b = 1.0 μm, and $\theta = 0.16°$ (resulting in the dislocation of point A in Fig. 5 for (1.0 μm, 1.0 μm), which represents the alignment precision of the experimental setup), the initial capacitance becomes 57.3 fF, 0.93% higher than that of the zero-misalignment assembly, indicating that this misalignment has a minimal effect on the capacitance value.

With the assumption that the Young's modulus of silicon is 150.0GPa [27], the spring constant of the top comb, k, is calculated to be 26.2 N/m. At an applied voltage of 70.0 V, the vertical displacement of the top comb is calculated to be 1.06 μm for the case of no misalignment. With the aforementioned misalignment parameters, the displacement is calculated to be 1.07 μm. The mass of the top comb, m, is calculated to be 2.82 ng, given its geometry (Table I) and the density of silicon (2.3290 g/cm^3). Thus, the resonant frequency of the top comb is calculated to be $f = \frac{1}{2\pi}\sqrt{\frac{k}{m}}$ =15.3 kHz.

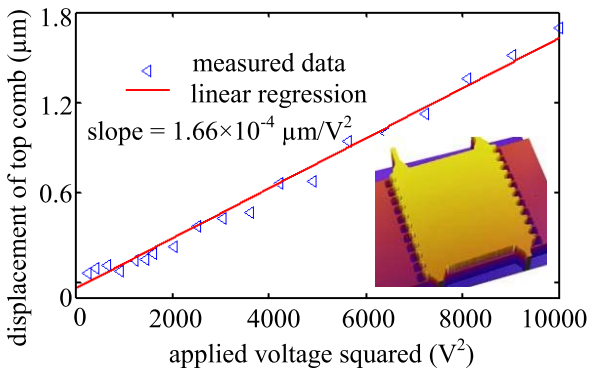

Fig. 7. Characterization of the comb drive as an actuator, with the resultant displacement of the top comb as a function of the applied voltage squared measured by an optical profiler. Inset shows the optical profiler image of the comb drive.

IV. Characterization of Assembled Comb Drive

To obtain the actual spring constant of the top comb, a nano-indenter (TI 950 Triboindenter, Hysitron) is used to push down the top comb and measure the resistance force. The indentation force as a function of the indentation depth is shown in Fig. 6(a), yielding a stiffness of 39.0 N/m. The inaccuracy from the calculated result (26.2 N/m) could be attributed to (1) the actual Young's modulus of the silicon is higher than the assumed value (150.0 GPa) [27], or (2) the actual thickness of the flexure beams is thicker than the designed value (5 μm) due to the microfabrication error.

To use the comb drive as a displacement or force sensor, the relationship between the capacitance change of the comb drive and the displacement of the top comb needs to be calibrated. To measure the capacitance change of the comb drive, the device is glued and wire bonded to a custom-made PCB with a capacitance-to-digital converter (AD7746, Analog Devices). The calibration results are shown in Fig. 6(b). Determined from the noise level of the readout voltage, the comb drive exhibits a displacement-sensing resolution of 0.17 μm and a force-sensing resolution of 6.63 μN at a sampling frequency of 10 Hz. If a higher displacement-sensing resolution is desired, the number or the length of the comb fingers can be increased, or the gap between the opposing comb fingers can be decreased.

The actuation function of the comb drive is also characterized, by applying a voltage to the comb drive and measuring the resultant displacement of the top comb using an optical profiler (NT1000, Veeco). The results are shown in Fig. 7. At an actuation voltage of 70.0 V, the displacement is measured to be 0.68 μm, smaller than the value from the theoretical calculation (1.07 μm) for a certain misalignment. The difference between the measured and calculated values is attributed to the aforementioned underestimated stiffness of the flexure beams.

The frequency response of the comb drive is also characterized, as shown in Fig. 8. A sinusoidal actuation voltage with an offset, expressed as $V(t) = 0.5 \times \sin(2\pi f_{\text{act}} t) + 0.5$, is applied to the top comb, while the bottom comb is grounded. The actuation frequency, f_{act}, is varied between

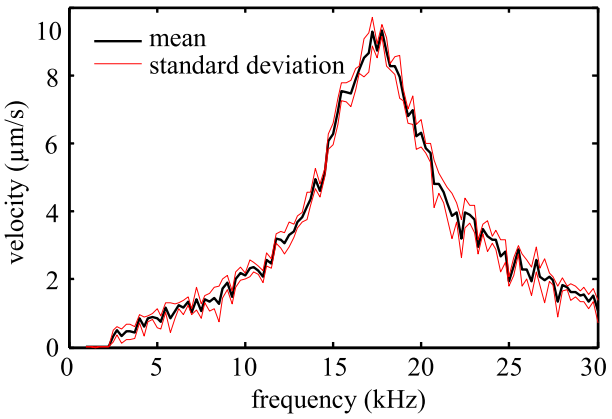

Fig. 8. Magnitude of the velocity of the top comb as a function of the frequency of actuation voltage. The mean (thick black curve) and standard deviation (thin red curves) of the velocity measured for 5 times are plotted. The resonant frequency of the structure is 17.6 kHz. The quality factor is 2.93.

1 kHz and 30 kHz. The magnitude of the actuation voltage is small in order for the comb drive to work in the linear range. The velocity of the structures is measured by a laser Doppler vibrometer (MSV-300, Polytec), with the magnitude of the velocity at the actuation frequency being obtained by a lock-in-amplifier (7280, Signal recovery). The maximum displacement at resonance is only 126 pm, ensuring the linear behavior of the comb drive. The resonant frequency is determined to be 17.6 kHz, which is larger than the calculated value (15.3 kHz), mainly due to the underestimation of the flexure beams's stiffness. The quality factor is determined to be 2.93.

V. Conclusion

Micro-masonry has herein been demonstrated to be a route to constructing MEMS devices that would be challenging or impossible to accomplish with monolithic microfabrication. Fragile as well as sturdy MEMS components were fabricated and assembled using an elastomeric microtipped stamp, followed by rapid thermal annealing for direct bonding. The assembled comb-drive device was characterized for its sensing and actuating capabilities. Future opportunities include optimizing device parameters and developing high-performance microdevices based on micro-masonry, such as microscale weight sensors [28], [29], micromirrors [22], [30], and vibration-driven energy harvesters [31], [32].

References

[1] K. Aoki, H. T. Miyazaki, H. Hirayama, K. Inoshita, T. Baba, K. Sakoda, N. Shinya, and Y. Aoyagi, "Microassembly of semiconductor three-dimensional photonic crystals," *Nature Mater.*, vol. 2, pp. 117–121, Jan. 2003.

[2] N. Dechev, W. L. Cleghorn, and J. K. Mills, "Microassembly of 3-D microstructures using a compliant, passive microgripper," *J. Microelectromech. Syst.*, vol. 13, no. 2, pp. 176–189, Apr. 2004.

[3] H. T. Miyazaki, Y. Tomizawa, S. Saito, T. Sato, and N. Shinya, "Adhesion of micrometer-size polymer particles under a scanning electron microscope," *J. Appl. Phys.*, vol. 88, no. 6, pp. 3330–3340, Jun. 2000.

[4] S. Saito, H. T. Miyazaki, T. Sato, and K. Takahashi, "Kinematics of mechanical and adhesional micromanipulation under a scanning electron microscope," *J. Appl. Phys.*, vol. 92, no. 9, pp. 5140–5149, Aug. 2002.

[5] Y. Zhang, X. Liu, C. Ru, Y. L. Zhang, L. Dong, and Y. Sun, "Piezoresistivity characterization of synthetic silicon nanowires using a MEMS device," *J. Microelectromech. Syst.*, vol. 20, no. 4, pp. 959–967, Aug. 2011.

[6] X. Ye, Y. Zhang, C. Ru, J. Luo, S. Xie, and Y. Sun, "Automated pick-place of silicon nanowires," *IEEE Trans. Autom. Sci. Eng.*, vol. 10, no. 3, pp. 554–561, Jul. 2013.

[7] J. D. Wason, J. T. Wen, J. J. Gorman, and N. G. Dagalakis, "Automated multiprobe microassembly using vision feedback," *IEEE Trans. Robot.*, vol. 28, no. 5, pp. 1090–1103, Oct. 2012.

[8] H. Xie and S. Regnier, "Development of a flexible robotic system for multiscale applications of micro/nanoscale manipulation and assembly," *IEEE/ASME Trans. Mechatronics*, vol. 16, no. 2, pp. 266–276, Apr. 2011.

[9] H. Xie and S. Regnier, "Three-dimensional automated micromanipulation using a nanotip gripper with multi-feedback," *J. Micromech. Microeng.*, vol. 19, no. 7, p. 075009, Jul. 2009.

[10] O. Fuchiwaki, A. Ito, D. Misaki, and H. Aoyama, "Multi-axial micromanipulation organized by versatile micro robots and micro tweezers," in *Proc. IEEE ICRA*, May 2008, pp. 893–898.

[11] D. Heriban and M. Gauthier, "Robotic micro-assembly of microparts using a piezogripper," in *Proc. IEEE/RSJ Int. Conf. Intell. Robot. Syst.*, Sep. 2008, pp. 4042–4047.

[12] W. Driesen, T. Varidel, S. Regnier, and J.-M. Breguet, "Micro manipulation by adhesion with two collaborating mobile micro robots," *J. Micromech. Microeng.*, vol. 15, no. 10, pp. S259–S267, Oct. 2005.

[13] K. Tsui, A. A. Geisberger, M. Ellis, and G. D. Skidmore, "Micromachined end-effector and techniques for directed MEMS assembly," *J. Micromech. Microeng.*, vol. 14, no. 4, pp. 542–549, Apr. 2004.

[14] M. Mayyas, P. Zhang, W. H. Lee, D. Popa, and J. C. Chiao, "An active micro joining mechanism for 3D assembly," *J. Micromech. Microeng.*, vol. 19, no. 3, p. 035012, Mar. 2009.

[15] S. Saito and M. Sonoda, "Non-impact deposition for electrostatic micromanipulation of a conductive particle by a single probe," *J. Micromech. Microeng.*, vol. 18, no. 10, p. 107001, Oct. 2008.

[16] D. S. Haliyo, S. Regnier, and J.-C. Guinot, "*mu*MAD, the adhesion based dynamic micro-manipulator," *Eur. J. Mech. A, Solids*, vol. 22, no. 6, pp. 903–916, Nov. 2003.

[17] Y. Zhang, B. K. Chen, X. Liu, and Y. Sun, "Autonomous robotic pick-and-place of microobjects," *IEEE Trans. Robot.*, vol. 26, no. 1, pp. 200–207, Feb. 2010.

[18] B. K. Chen, Y. Zhang, D. Perovic, and Y. Sun, "MEMS microgrippers with thin gripping tips," *J. Micromech. Microeng.*, vol. 21, no. 10, p. 105004, Oct. 2011.

[19] K. Kim, X. Liu, Y. Zhang, and Y. Sun, "Nanonewton force-controlled manipulation of biological cells using a monolithic MEMS microgripper with two-axis force feedback," *J. Micromech. Microeng.*, vol. 18, no. 5, p. 055013, May 2008.

[20] F. Beyeler, A. Neild, S. Oberti, D. J. Bell, Y. Sun, J. Dual, and B. J. Nelson, "Monolithically fabricated microgripper with integrated force sensor for manipulating microobjects and biological cells aligned in an ultrasonic field," *J. Microelectromech. Syst.*, vol. 16, no. 1, pp. 7–15, Feb. 2007.

[21] T. C. Duc, G.-K. Lau, J. F. Creemer, and P. M. Sarro, "Electrothermal microgripper with large jaw displacement and integrated force sensors," *J. Microelectromech. Syst.*, vol. 17, no. 6, pp. 1546–1555, Dec. 2008.

[22] E. Iwase, H. Onoe, K. Matsumoto, and I. Shimoyama, "Hidden vertical comb-drive actuator on PDMS fabricated by parts-transfer," in *Proc. IEEE MEMS*, Jan. 2008, pp. 116–119.

[23] H. Keum, A. Carlson, H. Ning, A. Mihi, J. D. Eisenhaure, P. V. Braun, J. A. Rogers, and S. Kim, "Silicon micro-masonry using elastomeric stamps for three-dimensional microfabrication," *J. Micromech. Microeng.*, vol. 22, no. 5, p. 055018, May 2012.

[24] S. Kim, J. Wu, A. Carlson, S. H. Jin, A. Kovalsky, P. Glass, Z. Liu, N. Ahmed, S. L. Elgan, W. Chen, P. M. Ferreira, M. Sitti, Y. Huang, and J. A. Rogers, "Microstructured elastomeric surfaces with reversible adhesion and examples of their use in deterministic assembly by transfer printing," *Proc. Nat. Acad. Sci. USA*, vol. 107, no. 40, pp. 17095–17100, Oct. 2010.

[25] D.-W. Oh, S. Kim, J. A. Rogers, D. G. Cahill, and S. Sinha, "Interfacial thermal conductance of transfer-printed metal films," *Adv. Mater.*, vol. 23, no. 43, pp. 5028–5033, Nov. 2011.

[26] J. Xie and Y. Zhu, "The calculation of capacitance and electric field for non-parallel plate capacitor," *Eng. Phys.*, vol. 9, no. 1, pp. 2–3, Jan. 1999.

[27] M. Hopcroft, W. Nix, and T. Kenny, "What is the Young's modulus of silicon?" *J. Microelectromech. Syst.*, vol. 19, no. 2, pp. 229–238, Apr. 2010.
[28] K. Park, L. J. Millet, J. Huan, N. Kim, G. Popescu, N. Aluru, K. J. Hsia, and R. Bashir, "Measurement of adherent cell mass and growth," *Proc. Nat. Acad. Sci. USA*, vol. 107, pp. 20691–20696, Nov. 2010.
[29] K. Park, N. Kim, D. T. Morisette, N. R. Aluru, and R. Bashir, "Resonant MEMS mass sensors for measurement of microdroplet evaporation," *J. Microelectromech. Syst.*, vol. 21, no. 3, pp. 702–711, Jun. 2012.
[30] D. Hah, S. T.-Y. Huang, J.-C. Tsai, H. Toshiyoshi, and M. C. Wu, "Low-voltage, large-scan angle MEMS analog micromirror arrays with hidden vertical comb-drive actuators," *J. Microelectromech. Syst.*, vol. 13, no. 2, pp. 279–289, Apr. 2004.
[31] P. D. Mitcheson, T. C. Green, E. M. Yeatman, and A. S. Holmes, "Architecture for vibration-driven micropower generators," *J. Microelectromech. Syst.*, vol. 13, no. 3, pp. 429–440, Jun. 2004.
[32] S. P. Beeby, R. N. Torah, M. J. Tudor, P. Glynne-Jones, T. O'Donnel, C. R. Saha, and S. Roy, "A micro electromagnetic generator for vibration energy harvesting," *J. Micromech. Microeng.*, vol. 17, no. 7, pp. 1257–1265, Jul. 2007.

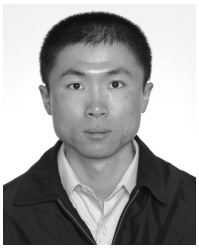

Yong Zhang received the B.S. and M.S. degrees in mechatronics engineering from the Harbin Institute of Technology, Harbin, China, in 2005 and 2007, respectively, and the Ph.D. degree in electrical and computer engineering from the University of Toronto, Toronto, ON, Canada, in 2011. He was a Post-Doctoral Fellow with the Department of Mechanical Science and Engineering, University of Illinois at Urbana-Champaign, Urbana, IL, USA, from 2011 to 2012. He is currently a Post-Doctoral Fellow with the School of Aerospace Engineering, Georgia Institute of Technology, Atlanta, GA, USA. His current research interests include the design and fabrication of MEMS devices, micro/nanomanipulation under optical and electron microscopy, and 3-D micro/nanomanufacturing.

Hohyun Keum received the B.S. degree in mechanical engineering from the University of Illinois at Urbana-Champaign, Urbana, IL, USA, in 2010, where he has been pursuing the Ph.D. degree since 2011. His current research interests include developing transfer printing micro-fabrication technique, which includes heterogeneous assembly, design and fabrication of MEMS device, and 3-D micromanufacturing.

Kidong Park received the B.S. degree in electrical engineering from Seoul National University, Seoul, Korea, in 1999, and the Ph.D. degree in electrical and computer engineering from Purdue University, West Lafayette, IN, USA, in 2009. From 2009 to 2010, he was a Post-Doctoral Research Associate with the Micro and Nanotechnology Laboratory, University of Illinois at Urbana-Champaign (UIUC), Urbana, IL, USA. From January 2011 to October 2011, he was with Samsung Electronics as a Senior Engineer. He is currently a Post-Doctoral Research Associate with the Micro and Nanotechnology Laboratory, UIUC. His current research interests include modeling, design, fabrication, and characterization of bio-MEMS sensors, and microfluidic devices for medical diagnostic and cellular studies.

Rashid Bashir received the B.S.E.E. degree from Texas Tech University, Lubbock, TX, USA, in 1987, and the M.S.E.E. and Ph.D. degrees from Purdue University, West Lafayette, IN, USA, in 1989 and 1992, respectively. From 1992 to 1998, he was with National Semiconductor, Analog/Mixed Signal Process Technology Development Group, as a Senior Engineering Manager. He joined Purdue University as an Assistant Professor in 1998 and became a Professor of electrical and computer engineering. Since 2007, he has been the Abel Bliss Professor of Electrical and Computer Engineering and Bioengineering, and the Director of the Micro and Nanotechnology Laboratory (a campus-wide clean room facility) with the University of Illinois at Urbana-Champaign, Urbana, IL, USA. He has authored or coauthored over 150 journal papers, over 160 conference papers and conference abstracts, over 100 invited talks, and has been granted 34 patents. He is a Fellow of APS, AIMBE, and AAAS. His current research interests include bionanotechnology, bioMEMS, lab on a chip, interfacing biology and engineering from molecular to tissue scale, and applications of semiconductor fabrication to biomedical engineering, all applied to solve biomedical problems.

Seok Kim received the B.S. and M.S. degrees from the Pohang University of Science and Technology, Pohang, Korea, and the University of California at Los Angeles, Los Angeles, CA, USA, in 2000 and 2005, respectively, and the Ph.D. degree from Carnegie Mellon University, Pittsburgh, PA, USA, in 2009. After a two-year post-doctoral career with the University of Illinois at Urbana-Champaign (UIUC), Urbana, IL, USA, he joined the Department of Mechanical Science and Engineering, UIUC, as an Assistant Professor, in 2011. His current research interests include biomimetic reversible dry adhesives, transfer printing-based microassembly, and MEMS fabrication technologies.